

Effect of manmade pixels on the inherent dimension of natural material distributions

Ariel Schlamm,^a David Messinger,^a and William Basener^b

^aRochester Institute of Technology, Center for Imaging Science, Digital Imaging and Remote Sensing Laboratory, 54 Lomb Memorial Drive, Rochester, NY, 14623, USA

^bRochester Institute of Technology, School of Mathematical Sciences, 85 Lomb Memorial Drive, Rochester, NY, 14623, USA

ABSTRACT

The inherent dimension of hyperspectral data may be a useful metric for discriminating between the presence of manmade and natural materials in a scene without reliance on spectral signatures taken from libraries. Previously, a simple geometric method for approximating the inherent dimension was introduced along with results from application to single material clusters. This method uses an estimate of the slope from a graph based on the point density estimation in the spectral space. Other information can be gathered from the plot which may aid in the discrimination between manmade and natural materials. In order to use these measures to differentiate between the two material types, the effect of the inclusion of manmade pixels on the phenomenology of the background distribution must be evaluated. Here, a procedure for injecting manmade pixels into a natural region of a scene is discussed. The results of dimension estimation on natural scenes with varying amounts of manmade pixels injected are presented here, indicating that these metrics can be sensitive to the presence of manmade phenomenology in an image.

Keywords: hyperspectral, inherent dimension

1. INTRODUCTION

Hyperspectral imagery typically has hundreds of bands of spectral data; therefore each image has hundreds of dimensions in some sense. It is assumed that the inherent dimension of the subject(s) is less than n , the number of bands recorded. Dimension reduction of an image to the estimated dimension, d , where $d < n$, of a spectral image is commonly used as a means to reduce processing time and improve algorithm results by transforming the data into d unique dimensions. This relies on the assumption that the entire spectral image is contained in the same d -dimensional subspace.¹

A spectral image rarely consists of a single type of landcover; often the subject matter is a combination of natural materials, including forest, grass, and water, and manmade materials, including buildings and roads. The individual spectra of these materials are not the same and neither are their distributions. Vegetation spectra are subject to natural variability while manmade materials are manufactured in a controlled environment to minimize variability. For these reasons, an estimate of the inherent dimension may be used to discriminate between natural and manmade materials.

The point density algorithm² is an approach to estimating the correlation dimension^{3,4} of a dataset. As the name implies, the point density algorithm in implementation considers the density of points within small elements, in this case spheres. These algorithms determine the dimension by its relation with the volume, V , of the space and the number of points, N_V , contained in the volume. The “volume” of a line is proportional to the length or radius r of that line. The “volume” of a circle is the area of the circle, or $\pi r^2 \propto r^2$. The volume of a

Further author information:

Ariel Schlamm.: E-mail: aas1510@cis.rit.edu

David Messinger: E-mail: messinger@cis.rit.edu

William Basener: E-mail: wfbsma@rit.edu

sphere is $\frac{4}{3}\pi r^3 \propto r^3$. It follows that the volume of a d -dimensional sphere is proportional to r^d . This is only true if the assumption in Equation 1,

$$V \propto N_V \propto r^d \rightarrow \log N_V \propto d \log r, \tag{1}$$

is made. For example, in a uniformly distributed space the number of points, N_V , is proportional to the volume, V . The dimension is estimated by calculating the slope of the line between the number of points within a radius and the radius itself.²

Implementation of this algorithm requires the assumption made in Equation 1, that the number of points contained in a volume is proportional to the volume itself. Figure 1(a) shows points uniformly distributed on a line. The Euclidean distance in the spectral space from the center of the line to all other points is calculated. The points within radii of increasing size are counted. The log-log plot of these values is produced in Figure 1(b) and the slope of the line is estimated to be the dimension.

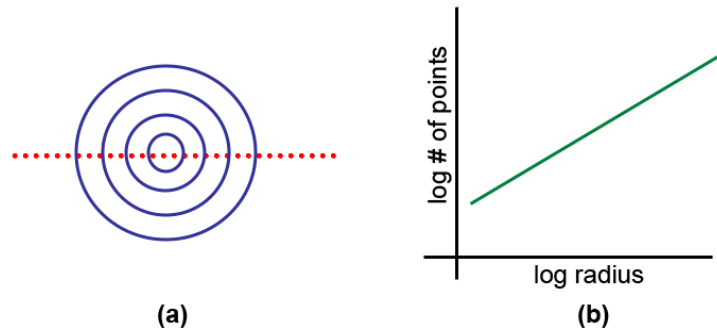


Figure 1. Illustration of counting the number of points within a 2D sphere and the resulting point density graph.

As real data is not uniformly distributed, the resultant plot does not generally look like Figure 1(b). The deviation from the ideal plot introduces other segments of the plot that can be measured. Section 2.1 introduces these other metrics that can be measured from the graph generated to estimate the dimension. An automated method to estimate these values is presented. Section 2 also describes the approach of using manmade pixel injection to test the use of estimated dimension as a metric on a hyperspectral scene. Section 3 presents the results applied to hyperspectral imagery of natural scenes with increasing proportions of manmade pixels included.

2. APPROACH

2.1 Estimated Metrics from the Point Density Plot

When the point density algorithm was previously introduced,^{2,5} it was shown that when applied to complex data, whether synthetic or real, linear regression was not an accurate method to estimating the slope of the resulting graph.

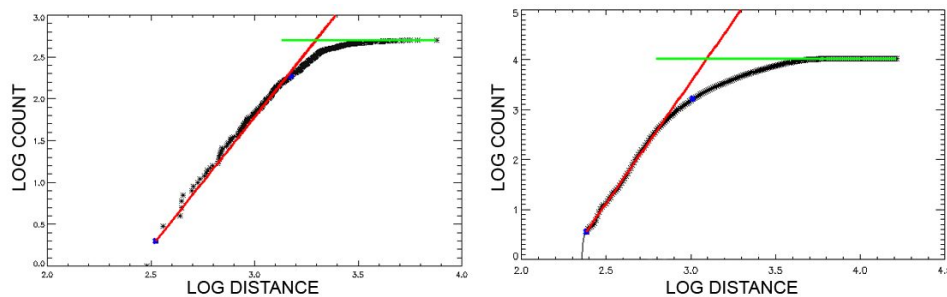


Figure 2. Examples of incline and tail on a plot created from real hyperspectral data of road (left) and forest (right).

Figure 2 shows two examples of the point density plot for a group of pure road pixels (left) and forest pixels (right). The plots have two distinct linear regions, demonstrated in Figure 3(left): a primary incline and a flat

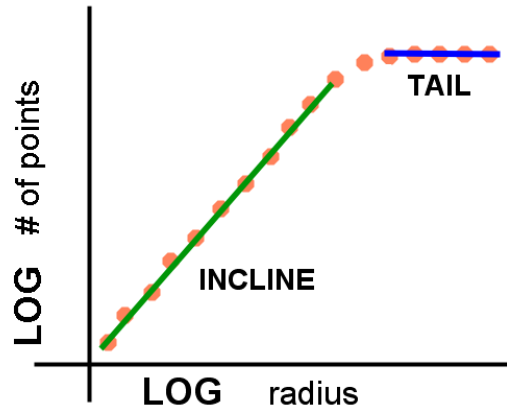


Figure 3. Left: Notional plot of a dimension estimation plot illustrating the incline and tail regions.

tail. These two regions lead to two distinct metrics that can be estimated from the plot, the slope and the tail length. The slope of the incline portion of the plot is an estimation of the dimension around the center or highly populated part of the data cloud. This estimate of dimension excludes influence from anomalies and others points at a large distance from the cluster center. The flat tail of the plot comes from relatively few points in the hyperspace at large distances from the center. The length of this tail corresponds to the range in spectral space in which the spectrally distant points fall. If the length of the tail is short, there are few pixels at a large distance from the cluster, which may indicate a more pure material. If a long tail is present, there are many pixels at a large distance from the center. This may be evidence of a secondary cluster of points, far from the centroid, or many small or singleton anomalies in the sample.

An automated method to measure the slope of the incline portion and the tail length was developed. The points on the flat tail are identified by casting a zero slope line at the y-axis value of the last points on the graph and choosing those points with a small RMS error from the line. The length of this line is calculated over the range of data that “fit” the horizontal line. The tail points are not considered when calculating the slope of the incline. To estimate the best fit slope of the incline, a straight line is drawn from the first point in the graph to a random midpoint and the RMS error between the line and points is calculated. The error function is minimized to find the best fit line to the incline points from which to estimate the slope.

Between the incline and flat tail is a transition region. This transition may occur over a very short change or a large range in radii, shown in Figure 2. The plot generated from road pixels, a pure material, has a very short transition, while the same plot generated from forest pixels, which may include different species of trees, exposed terrain below the canopy, and shadow, has a long transition. Instead of measuring this transition directly, the error of the data to the piece-wise fit of the two lines found in the automated fitting method can also be used as a metric. Examples of the error of the point density plot to a piece-wise fit to the plot is shown in Figure 4 for the two graphs from Figure 2. The process taken to gather the three metrics is shown in Figure 5. If the error to the piece-wise function is small, the data fit well to the two lines and there is a very short transition region. This may also indicate a pure material. If the error is large, the transition region is large and the data are likely cluttered with a variety of materials. This itself may not indicate manmade material as an area cluttered with natural materials can also have a high error. In either case, the relationship between the incline and tail regions is a direct measure of the distribution of the data in the spectral hyperspace. This will continue to be investigated and utilized in future work.

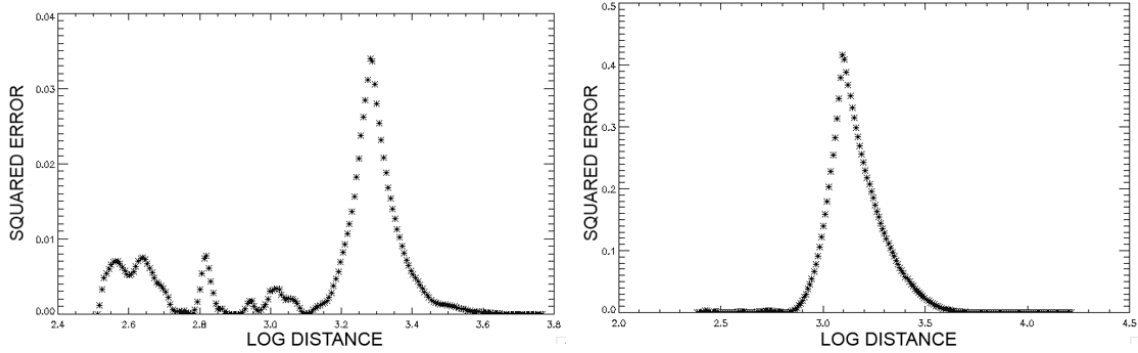


Figure 4. Total squared error to the piece-wise fit of the point density plots from Figure 2. road (left) and forest (right). Note the difference in the squared error scale.

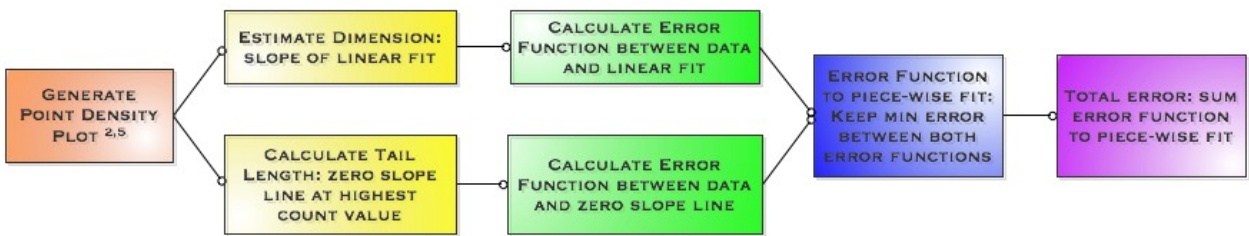


Figure 5. Process used to determine the three metrics.

2.2 Pixel Injection

To test the accuracy of using the described metrics to identify the presence of manmade materials in a predominantly natural scene, similar natural scenes with and without manmade materials are required. Three tiles, with approximately 10,000 pure natural material pixels each, were selected from a HyMAP reflectance hyperspectral data set of Cooke City, MT, shown in Figure 6.⁶ The presence of manmade pixels must be simulated in these tiles, either in full pixels or at the subpixel level. Cafer, et al. (2007) present a subpixel target implantation method which takes manmade material spectra from a library and mixes them with in-scene pixels.⁷ In our case, manmade pixels in downtown Cooke City, including various buildings, parking lots, and cars, were selected from the same dataset as the tiles and put into a library of 2333 manmade pixels. Taking manmade pixels from the same scene guaranteed the spectra were all in the same units and had gone through the same atmosphere and calibration. These manmade spectra were used to replace spectra in the natural tiles so there were full pixel manmade materials in the scene. Figure 7 shows the average spectrum of the three natural tiles and the average spectral of the manmade material spectral library. Three different natural regions, shown in Figure 6 as forest, grass, and foothills, were used as the base tiles. In order to observe how the dimension changes as more manmade pixels are included in the scene, an increasing number of random pixels in the natural tiles were replaced with random manmade spectra taken from the library. At every increment of the number of manmade pixels, 200 random trials of the pixel injection were done, resulting in 200 estimates of each metric for each percentage of manmade pixels.

3. RESULTS

Figure 8 shows the mean estimated dimension and the mean line fitting error of 50 and 200 trials for the forest scene on the same plot. As manmade pixels are added to the scene, the dimension is increasing and the error is relatively constant. At approximately 15% manmade pixels there is a spike in both the dimension and error graphs. When the error is high, it indicates that the point density graph does not fit well to the linear piece-wise function, so the dimension estimated is no longer considered accurate. Typically, the piece-wise function has

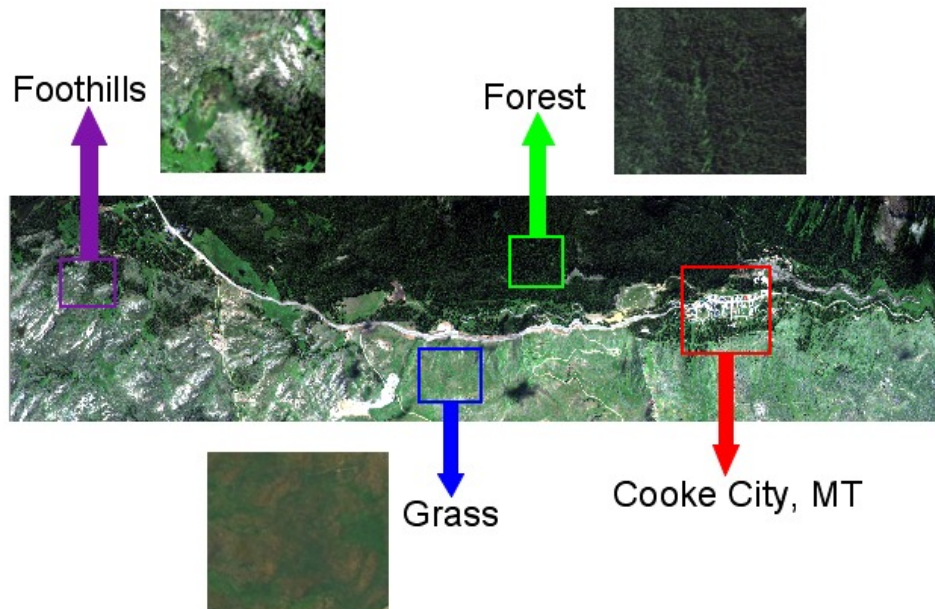


Figure 6. Visible image of HyMAP collection over Cooke City, MT with the three natural tiles selected. (for color images, please see electronic version of paper)

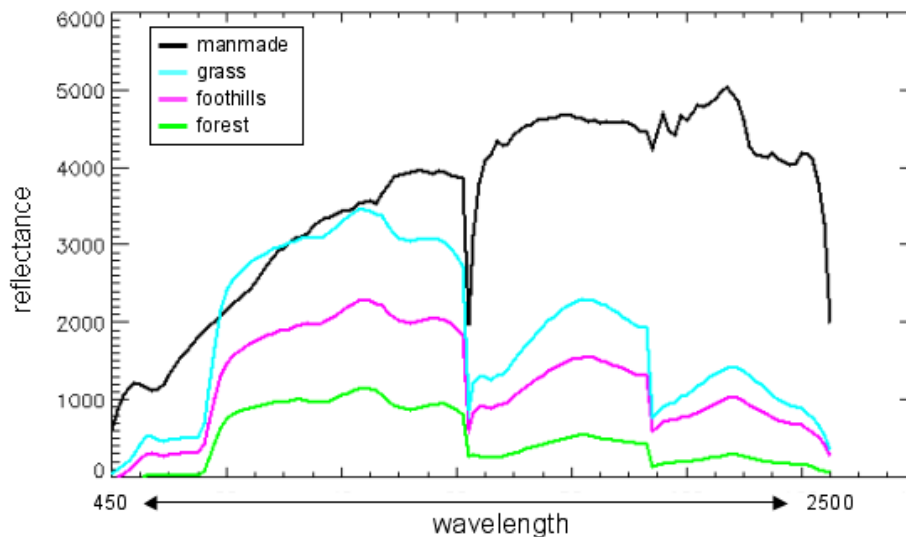


Figure 7. Average reflectance spectra of forest (green), grass (cyan), foothills (magenta), and city (black) regions used in this analysis. (for color images, please see electronic version of paper)

a poor fit when the point density plot has no linear incline and only a transition region and flat tail which presents as an increasing curve with decreasing slope. Adding a significant portion of manmade pixels to the forest increases the clutter substantially and an accurate dimension estimation cannot be made due to the multi-material clutter. For this reason, the remaining graphs only display up to 15% manmade pixels injected. Note that this effect was observed in the forest tile and the physical cause is under further investigation. The mean estimated metric of 200 trials is displayed on all plots. The results for dimension, tail length, and fitting error

as a function of the percentage of manmade pixels in the tile are presented here.

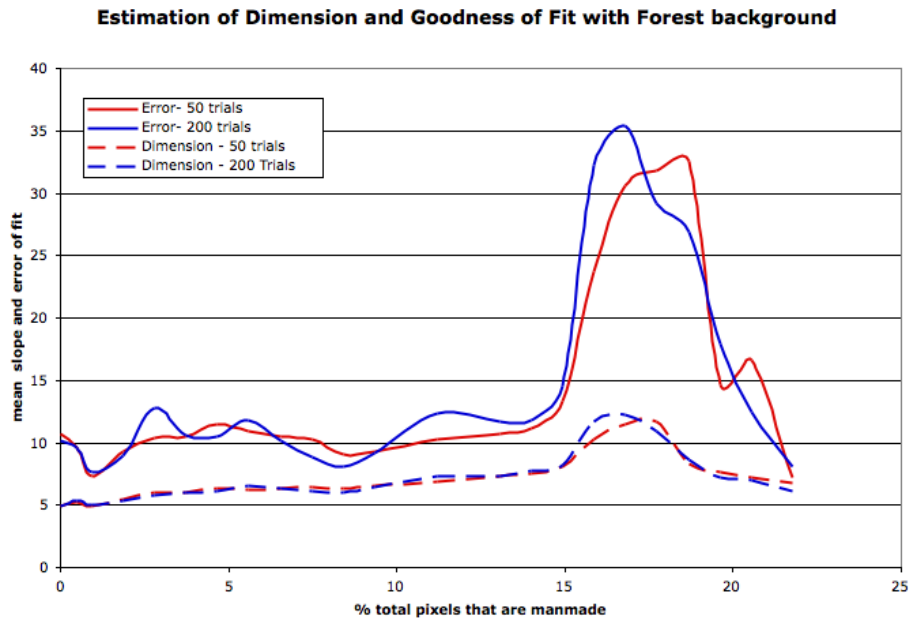


Figure 8. Dimension and error of linear piece-wise fit as a function of percentage of manmade pixels included in a forested region.

Figure 9 shows the mean estimated dimension as a function of percentage of manmade pixels in the tile. The dots on the y-axis show the dimension of the hyperspectral tiles with no manmade materials and the estimated dimension of the library of manmade materials. In general, the more manmade spectra added to the tile, the higher the estimated dimension. The foothills is the most cluttered region before the manmade materials are added and as a result it takes a larger number of manmade pixels until the dimension increases significantly.

The tail length as a function of the percentage of manmade materials is shown in Figure 10. In this case, the trend for each tile is identical. When just a few manmade pixels are added to the tiles, they are at a large distance from the center of the distribution, and therefore lengthen the tail of the point density plot. As more manmade pixels are added, the center of the distribution is pulled towards the manmade pixels and the tail length starts to shorten again.

Another effect of adding a significant number of manmade pixels is the lengthening of the transition region and increase in the line fitting error, shown at the higher percentages of manmade pixels in Figure 11. The line fitting error is initially lower for the forest region than the grass or foothills, which are both more cluttered tiles, and continues to be lower with increasing numbers of manmade pixels.

4. CONCLUSION

The use of the point density algorithm to estimate inherent dimension of hyperspectral data was extended to estimation of two additional metrics, flat tail length and line fitting error, that may be useful in discriminating between regions of natural materials and those that contain manmade materials. An automated linear piece-wise fitting procedure was introduced to measure the length of the flat line portion of the plot and the best fit slope of the incline portion of the point density plot. Three natural material regions, with varying degrees of clutter, from a single wide area scene were selected for analysis of the effect of manmade pixels on the three discrimination metrics. In general, the dimension increased as manmade pixels were added to the natural scenes when the two component model was a good fit to the data. The tail length of the scenes with manmade pixels added was significantly higher than the all natural scenes, even with only a handful of manmade pixels included in the tiles.

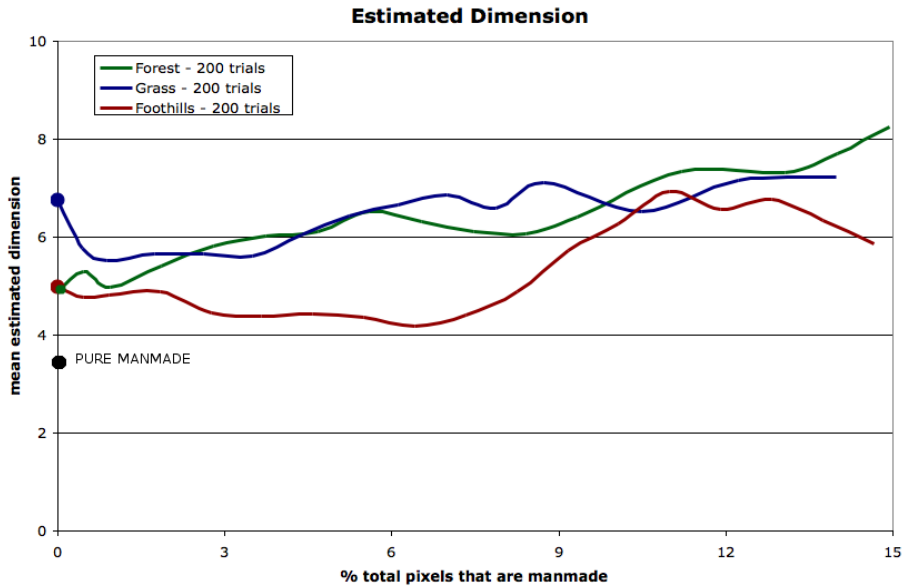


Figure 9. Estimated dimension as a function of percentage of manmade pixels for three natural regions.

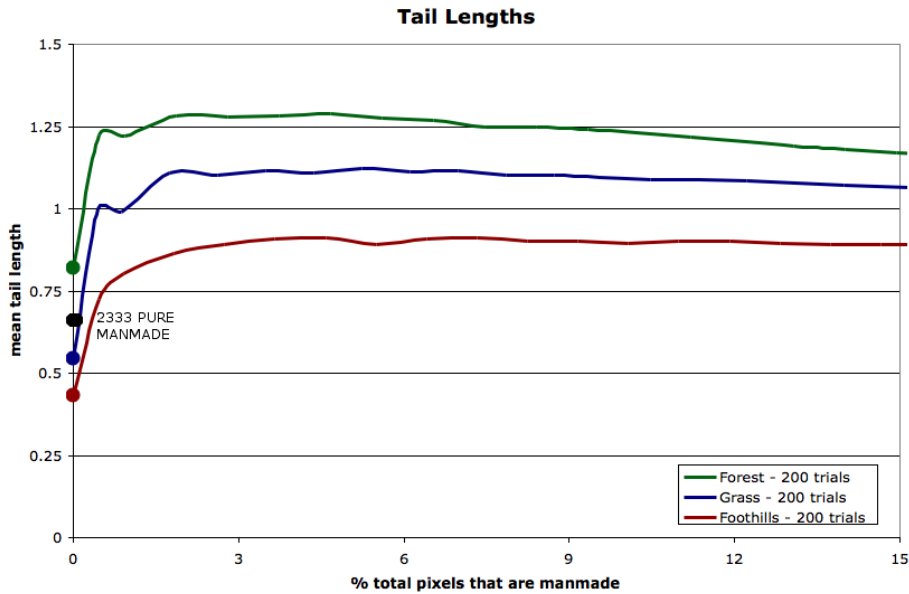


Figure 10. Dimension estimation plot tail length as a function of percentage of manmade pixels for three natural regions.

The line fitting error provides a measure of how accurate the piece-wise linear fit to the point density plot and how cluttered the scene may be. In the future, measuring the tail length as a method of detecting change in predominantly natural hyperspectral scenes will be investigated. Dimension, tail length, and total error will be further investigated for use in describing the data in the hyperspace and discriminating between pure and mixed materials image tiles.

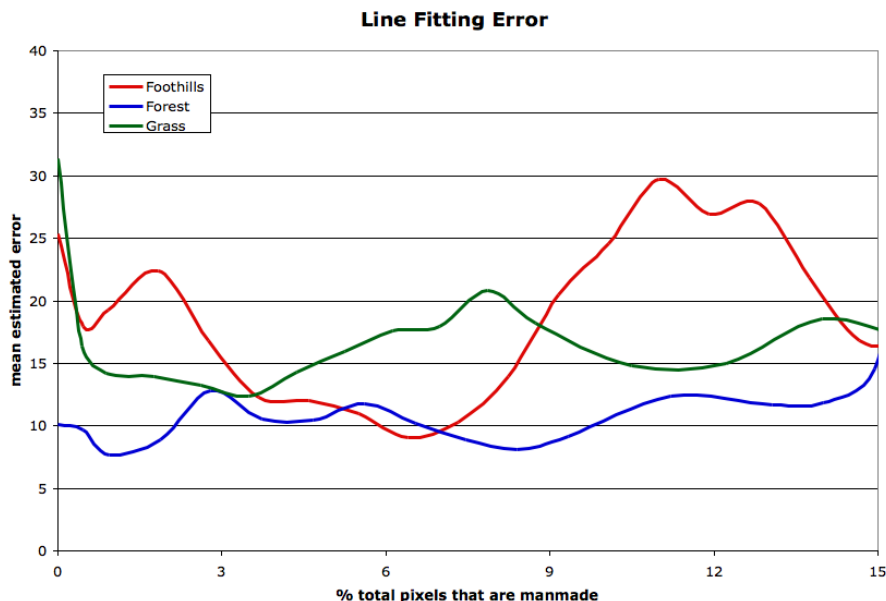


Figure 11. Error of linear piece-wise fit to dimension estimation plot as a function of percentage of manmade pixels included in three natural regions.(for color images, please see electronic version of paper)

ACKNOWLEDGMENTS

The authors wish to thank to John Kerekes for providing the HyMAP imagery of Cooke City, MT.

REFERENCES

- [1] Kirby, M., [*Geometric Data Analysis: An Empirical Approach to Dimensionality Reduction and the Study of Patterns*], 8–11, John Wiley & Sons, INC (2001).
- [2] Schlamm, A., Messinger, D., and Basener, B., “Geometric estimation of the inherent dimensionality of a single material cluster in multi- and hyperspectral imagery,” in [*Algorithms and Technologies for Multispectral, Hyperspectral, and Ultraspectral Imagery XII*], Shen, S. S. and Lewis, P. E., eds., *Proc. SPIE* **6966** (2008).
- [3] Grassberger, P. and Procaccia, I., “Characterization of strange attractors,” *Phys. Rev. Lett.* **50**, 346–349 (January 1983).
- [4] Theiler, J., “Estimating fractal dimension,” *J. Opt. Soc. Am.* **7**, 1055–1073 (June 1990).
- [5] Schlamm, A., Messinger, D., and Basener, W., “Geometric estimation of the inherent dimensionality of a single and multi-material clusters hyperspectral imagery,” Accepted for publication in JARS (Feb 2009).
- [6] Snyder, D., Kerekes, J., Fairweather, I., Crabtree, R., Shive, J., and Hager, S., “Development of a web-based application to evaluate target finding algorithms,” in [*IEEE Trans. Geosci. Rem. Sens.*], (2008).
- [7] Caefer, C. E., Stefanou, M. S., Nielsen, E. D., Rizzuto, A. P., and Rotman, S. R., “Analysis of false alarm distributions in the development and evaluation of hyperspectral point target detection algorithms,” *Optical Engineering* **46** (July 2007).